Changes Over Time in the Electrode/Brain Interface Impedance: An Ex-Vivo Study

Changes over Time in the Electrode/Brain Interface Impedance: An Ex-vivo Study

Leonardo Iannucci*, *Member, IEEE,* Gian Luca Barbruni*, *Graduate Student Member, IEEE,* Diego Ghezzi, *Senior Member, IEEE,* Marco Parvis, *Fellow, IEEE,* Sabrina Grassini, *Senior Member, IEEE,* and Sandro Carrara, *Fellow, IEEE,*

***Abstract*—Closed-loop neural implants based on continuous brain activity recording and intracortical microstimulation are extremely effective and promising devices to monitor and address many neurodegenerative diseases. The efficiency of these devices depends on the robustness of the designed circuits which rely on precise electrical equivalent models of the electrode/brain interface. This is true in the case of amplifiers for differential recording, voltage or current drivers for neurostimulation, and potentiostats for electrochemical bio-sensing. This is of paramount importance, especially for the next generation of wireless and ultra-miniaturised CMOS neural implants. Circuits are usually designed and optimized considering the electrode/brain impedance with a simple electrical equivalent model whose parameters are stationary over time. However, the electrode/brain interfacial impedance varies simultaneously in frequency and in time after implantation. The aim of this study is to monitor the impedance changes occurring on microelectrodes inserted in ex-vivo porcine brains to derive an opportune electrode/brain model describing the system and its evolution in time. In particular, impedance spectroscopy measurements have been performed for 144 hours to characterise the evolution of the electrochemical behaviour in two different setups analysing both the neural recording and the chronic stimulation scenarios. Then, different equivalent electrical circuit models have been proposed to describe the system. Results showed a decrease in the resistance to charge transfer, attributed to the interaction between biological material and the electrode surface. These findings are crucial to support circuit designers in the field of neural implants.**

***Index Terms*—Electrode/Brain Interface; Electrochemical Impedance Spectroscopy; Electrical Equivalent Circuit; Microelectrodes; Closed-loop Neural Implants; Neural Recording; Neurostimulation.**

Manuscript received Month X, 2023; revised Month X, 2023; accepted Month X, 2023. Date of publication Month X, 2023; date of current version Month X, 2023.

*Leonardo Iannucci and Gian Luca Barbruni have contributed equally to the paper. Corresponding author: Gian Luca Barbruni.

Leonardo Iannucci and Sabrina Grassini are with Department of Applied Science and Technology, Politecnico di Torino, Turin, Italy. (e-mail: leonardo.iannucci@polito.it; sabrina.grassini@polito.it)

Gian Luca Barbruni is with Bio/CMOS Interfaces Laboratory (BCI), École Polytechnique Fédérale de Lausanne, Neuchâtel, Switzerland and Medtronic Chair in Neuroengineering, École Polytechnique Fédérale de Lausanne, Geneva, Switzerland. (e-mail: gianluca.barbruni@epfl.ch)

Diego Ghezzi is with Medtronic Chair in Neuroengineering, École Polytechnique Fédérale de Lausanne, Geneva, Switzerland (e-mail: diego.ghezzi@epfl.ch)

Marco Parvis is with Department of Electronics and Telecommunications (DET), Politecnico di Torino, Turin, Italy. (e-mail: marco.parvis@polito.it)

Sandro Carrara is with Bio/CMOS Interfaces Laboratory (BCI), École Polytechnique Fédérale de Lausanne, Neuchâtel, Switzerland. (e-mail: sandro.carrara@epfl.ch)

Color versions of one or more of the figures in this article are available online at https://ieeexplore.ieee.org.

Digital Object Identifier 10.1109/TBCAS.2023.XXXXXXX

I. Introduction

ELECTRODE/brain interface impedance is of paramount importance for neural interfaces to record the brain activity [1], [2], to perform electrochemical biosensing [3, 4, 5], or to stimulate neural cells [6], [7]. The electrode/brain interfacial impedance depends on several factors, such as the electrode area and material, and the implant location [8]. Nowadays, penetrating microelectrodes are preferred with respect to planar electrodes. As an example, Utah-array based systems have been extensively used in both non-human primates [9], [10] and humans [11] for both neural recording and stimulation.

A. Recording

In neural recording, monitoring the electrochemical impedance stability of the microelectrodes is crucial to correctly acquire and process neural signals [12]. Intracortical microelectrodes are characterised by a small exposed and conductive tip. The smaller the exposed area, the higher the specificity of the neural recording, but the higher the electrode/brain impedance [13]. In principle, the activity of a single neuron can be monitored using microelectrodes with a size of the same order of magnitude. At the same time, being the interface area significantly reduced, the interaction with biological material strongly affects the overall impedance of the interface. Additionally, the electrode/brain impedance significantly impacts on the quality of neural recordings. In particular, the impedance changes affect the amount of noise that is introduced into the recording [14].

B. Stimulation

Intracortical stimulation using penetrating microelectrodes presents several advantages compared to surface stimulation [15]. Among the others, the spatial selectivity is increased and the injected charge can be reduced (i.e. tens of μA) avoiding strong current release, which may cause seizure in patients [16]. As for neural recording, the electrochemical impedance stability is fundamental in neurostimulation to deliver the necessary charge to the brain to have a safe and efficient therapy. Moreover, the electrode/brain interface impedance is markedly affected by charge injection [17]. Current pulses are able to remove, at least partially, the encapsulation tissue formed at the interface with the electrode, leading to a temporary decrease in the measured impedance [18]. This effect has a short duration, as generally the impedance is expected to increase again after

few hours [19, 20]. The rationale of this phenomenon is related to the ability of current pulses to remove cells adhered to a metallic substrate, even after applying the signal for few tens of seconds [21].

Recent advances in wireless power transmission techniques [22] and circuit design allow the miniaturisation of both neural implants and interfaces. This is extremely advantageous since electronics can be interfaced with much smaller brain areas, significantly increasing the specificity of the neural devices. However, with miniaturised CMOS electronics and constrained energy budget [23], [24] considering the most appropriate electrode/brain electrical equivalent circuit model is crucial for a robust and effective CMOS design [25]. These models [26], [27], [28] are used as circuital loads during the microelectronic design procedure of both neural amplifiers [29], voltage-mode [30], and current-mode [31] drivers for neurostimulators. The circuits are therefore designed to work under precise load conditions, usually derived by experimental measurements.

Typically, Randles-models (i.e., R-RC circuit) are used to characterize the electrode/brain interface impedance. The parameters are either calculated solving equations [32], fitting experimental data [33] or also estimated using numerical analysis approaches [34]. In all the cases, the selected models are considered stationary and the calculated values for the model parameters are usually considered time-invariant.

Indeed, among all the possible failure modes [35], the electrode/brain impedance variation in time is known as one of the failure causes for neural implants, which are then no more capable of correctly recording neural signals or delivering the adequate charge for an efficient neuromodulation therapy [36], [37]. As a matter of fact, during the lifetime of the neural implant, the impedance at the interface is not stationary in time [8]. Different variations occur both immediately after insertion (i.e. in the first days after implantation) and in the following weeks. Different studies have monitored the neural implant impedance both in the early post-operative phase and in the long term [38, 39]. Among them, many studies have reported a downward drift in the electrode impedance occurring in the first days after implantation [40, 41]. This phenomenon was attributed to the cerebrospinal fluid accumulation in the region closer to the implanted electrode [42]. After this early post-operative phase, a new increase in electrode impedance is generally expected due to the foreign body response, which leads to the formation of an encapsulation layer [20, 43]. Thickness and conductivity of the encapsulation layer affect the charge transfer phenomena at the interface between the electrode and the tissue, changing the impedance that the neural implant has to work with [44].

In summary, the several equivalent circuits at present in use in CMOS design for neural implant not necessarily correctly account for all the above-mentioned phenomena and they are not necessarily adapted to the modern microelectrodes. The aim of this work is then to derive robust models based on equivalent electrical circuits to describe the interface between the brain and the penetrating Pt/Ir microelectrodes, suitable for both neural recording and chronic stimulation. Here, we highlight that those models are not stationary and that the parameters are also varying considerably over time. We calculated for the first time the parameters considering their variation over time. Two different experimental setups were used. With the first one we determined the most appropriate equivalent electrical circuit under an ideal configuration for electrochemical analysis, extensively used nowadays in neuroscience. Then, the second setup was used to validate the proposed model with the gaze turned toward the next generation of wireless, free-floating and ultra miniaturised neural implants. This aspect is crucial for the design of robust circuits which are supposed to work at the electrode/brain interface.

The systems have been characterised ex-vivo for 144 hours, which is a sufficient time-frame to analyse the predominant changes on the interfacial impedance occurring immediately after implantation [42, 45]. In particular, the impedance variations occurring in the first days are attributed to the interaction between the electrode and the surrounding environment, constituted by inorganic ions and biological matter (such as proteins and cells). Impedance changes occurring after this time frame are generally related to the encapsulation phenomena, which can not occur in an ex-vivo test. Indeed, ex-vivo studies are flexible, easy to control and characterise and simpler to implement than in-vivo studies. However, it is worth noting that the results might not faithfully characterise what would happen in vivo, since there is no active blood flow (and no constant plasma extravasation) and no physiological micromotion. At the same time, even if not all biological phenomena are reproduced in ex-vivo studies, they still allow to study the changes over time in the electrode/brain interface impedance due to the interaction of the electrode with biological material and to derive general models considering the described phenomena to design more robust circuits.

II. Materials and Methods

A. Materials

In this study, Pt/Ir microelectrodes have been used (PI20030.5A3, Microprobes). They are 2-inch monopolar microelectrodes, coated by a 3-μm layer of Parylene-C and with an exposed tip of 25 μm. The microelectrode diameter is equal to 81 μm in the shaft and 3 μm on the tip, which has a taper ratio of about 25:1 and an area of 275 μm^2. The electrical connection between the microelectrode and the instrumentation is made using the male prepared gold pin connector (positioned at the end of the electrode opposite to the tip), which has been mounted to its female-to-BNC cable.

Ex-vivo porcine brains are demonstrated to be similar to human brains in terms of mechanical properties [46] and microstructures [47]. Therefore, fresh adult porcine brain were used, without any treatment, as in [48]. Porcine brains were dissected in almost 3-cm-thick slices obtaining several porcine brain samples. Each experiment was carried out in a separate plastic vial containing the porcine brain sample, in which the microelectrode was inserted from the top. Microelectrodes were deeply inserted into porcine brain samples for 2-3 mm to avoid brain surface inhomogeneities. Finally, the vial was filled with artificial cerebrospinal fluid (a-CSF) to have the electrolyte necessary for electrochemical measurements. The

Table I: aCSF COMPOSITION.

Compound	g/L
Albumin	0.2
Glucose	0.6
NaCl	6.78
KCl	0.216
$NaHCO_3$	1.764
$CaCl_2$ x $2H_2O$	0.735

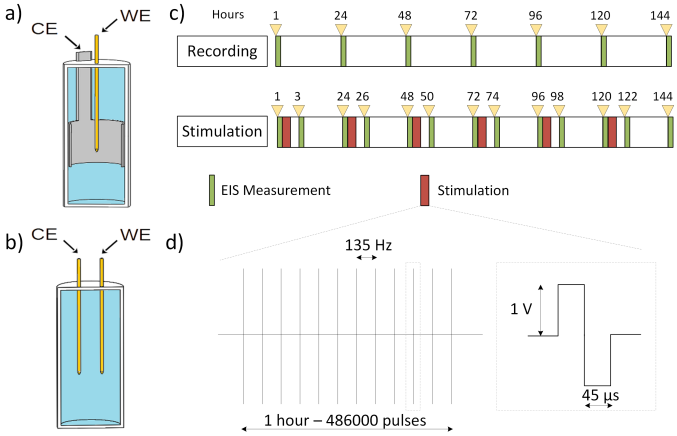

Figure 1: a) Scheme of the experimental setup A where the electrochemical cell is composed by the microelectrode (in yellow) as working electrode (WE) and the titanium foil (in gray) as counter electrode (CE). b) Scheme of the experimental setup B where the working and counter electrodes are represented by two identical microelectrodes (in yellow). The aCSF fills the plastic vials in light blue while the porcine brain is not represented for simplicity. (c) Graphical timely representation of the different experiments representing the recording and the chronic stimulation highlighting the EIS measurements and the stimulation periods. (d) Representation of the voltage-controlled biphasic neurostimulation waveform.

a-CSF has been prepared as in Table I, obtaining a solution with a measured $pH = 7.2$, as previously described [49, 50, 51, 52].

All tests were carried out at $37°C$ ($\pm 1°C$), positioning the vials in a temperature-controlled water bath (JB Aqua 2 Grant).

B. Test protocols and characterizations

The interface between the microelectrode and the porcine brain was characterized by Electrochemical Impedance Spectroscopy (EIS) measurements, performed once a day (i.e., each day at the same time) for 144 hours after the microelectrode insertion in the porcine brain. Electrochemical measurements were carried using an Ivium CompactStat.e 10800 electrochemical interface. EIS measurements were performed in a two-electrode cell, in the frequency range from 10^5 Hz to 10^{-1} Hz, using an alternating stimulus of 20 mV and acquiring 10 points per frequency decade. No DC bias was used in the EIS measurements. The investigated frequency range was chosen to characterise the interface between the biological environment and the electrode, without the influence of the tissue itself, which would affect the impedance spectra at higher frequencies [53, 54, 55]. To recreate the actual working environment of the neural implant, a two-electrode configuration was utilized instead of the traditional three-electrode electrochemical cell. In this two-electrode cell, recording and stimulation are differentially conducted between the two electrodes, without the application of reference potential nor system bias.

Two different setup were used, which will be referred to below as setup A and B (Figure 1-a,b). In setup A, the electrochemical cell was composed by a microelectrode (working electrode - WE) and a titanium foil with an area of 6 cm^2 (counter electrode - CE). The CE has a large surface area and thus its impedance is negligible compared to the WE one. Setup A is closer to conventional systems adopted for neural recording with multiple electrodes, such as the Utah array system [56]. In this case the CE is a large electrode which does not affect the WE recording. Indeed, in this two-electrode system, the measured impedance is related only to the WE and not to the CE. Therefore, setup A is also optimal for the electrochemical characterisation of the system.

In setup B two identical microelectrodes were inserted in the porcine brain. The first one is used as WE and the other one as CE (i.e. without the titanium foil). The distance between the two microelectrodes was 3 mm. Setup B is investigated with the gaze turned toward the next-generation implantable neural systems. In this case multiple miniaturised and wirelessly powered CMOS implants are integrated with a couple of microelectrodes to perform neural recording [24], [23], [57]. Setup B is more complex because the two microelectrodes have similar impedance and, therefore, are both subject to the interaction with the biological environment. Both the setups were used to analyse the impedance variation of a neural implant used for neural recording. The microelectrodes were inserted in the porcine brain for a total of 144 hours and characterised by EIS measurements acquired every 24 hours.

From the experimental results of the setup A, an Equivalent Electrical Circuit (EEC) model was derived to describe the impedance variation of the single microelectrode in the different phases of the experiments. The proposed model was then validated replicating the experiment with the setup B, where the impedance variation takes into account both the microelectrodes. EEC fitting was performed using the IviumSoft software.

The setup A was also used to study a relevant case for chronic neurostimulation. The microelectrodes were inserted in porcine brain tissue for 144 hours and stimulated for one hour every 24 hours. EIS measurements were acquired every 24 hours and also one hour after the end of the stimulation protocol. All test conditions are summarised in the timely scheme of Figure 1-c.

The stimulation pattern has been selected following the same parameters used in a previous in-vivo study involving Pt/Ir microelectrodes for deep brain stimulation [20]. The neurostimulation protocol is based on an anodic-first biphasic voltage-controlled pulse with an amplitude of 2 V_{pp} at zero off-

set (i.e., voltage-balanced), a stimulation frequency of 135 Hz and two equal phases of 45 μs each (Figure 1-d). Even if the peak-to-peak amplitude of this voltage-controlled stimulation pattern exceeds the water window of the Pt alloy (-0.6 V to +0.9 V [58]), it has been used in previous studies involving Pt/Ir microelectrodes [20, 18]. The neurostimulation protocol was applied continuously for one hour (i.e., 486000 biphasic pulses) using a waveform generator (Keysight 33500B Series).

At least three independent samples were investigated for each test condition.

After the test, all the microelectrodes were extracted from the biological tissue, gently rinsed in distilled water and ethanol and then dried in air. The tip morphology was then characterized by means of Scanning Electron Microscopy (SEM) using a Philips XLF-30. The microelectrodes were analysed without any additional sample preparation or cleaning. SEM characterization was performed acquiring secondary electrons using an accelerating voltage of 5 kV and an aperture size of 30 μm.

III. Results and Discussion

A. Impedance variation during Recording - Setup A

The setup A is used to carry out a first set of experiments to study the interfacial impedance of a single microelectrode using a large ring-shaped counter electrode. Figure 2 shows, as Bode diagram, the impedance modulus (a) and phase (b) measured on one representative WE which has been inserted into the porcine brain for 144 hours and characterised daily by EIS. The interaction between the Pt/Ir microelectrode and the surrounding environment has a major influence on the interfacial impedance. At the beginning of the experiment, the impedance spectrum is characterized by an high impedance modulus, which reaches about $4 \cdot 10^8$ Ω at frequencies smaller than 1 Hz. The behaviour is capacitive at higher frequencies, as can be observed from the phase values which remain close to $-90°$ until 30 Hz and then approach to $0°$ in the last frequency decades. It is worth noting that, even if multiple measurements were averaged to reduce the low-frequency noise, some spectra are characterised by a high impedance modulus (i.e., in particular at 1-hour), and the input-referred noise voltage of the built-in amplifier of the instrument is influencing the quality of the signal.

Remaining in contact with the biological tissue, the interface changes during the experiment, leading to a progressive decrease in the impedance modulus in a large frequency range, and predominantly in the low-frequency region (Figure 2-a). Already after 24 hours in contact with the animal tissue, the impedance modulus at the lowest analysed frequency decreases of more than one order of magnitude (i.e. from $4{\cdot}10^8$ Ω to $3{\cdot}10^7$ Ω). After 72 hours it stabilizes close to 10^5 Ω. These changes are also clearly visible in the phase diagram (Figure 2-b) where all the measurements after 72 hours remain below $-45°$ in almost the whole investigated frequency range (i.e. already from 10-30 kHz).

The modifications in the impedance spectra can be explained considering the state-of-the-art literature about the interaction between metal substrates and biofilms [59, 60].

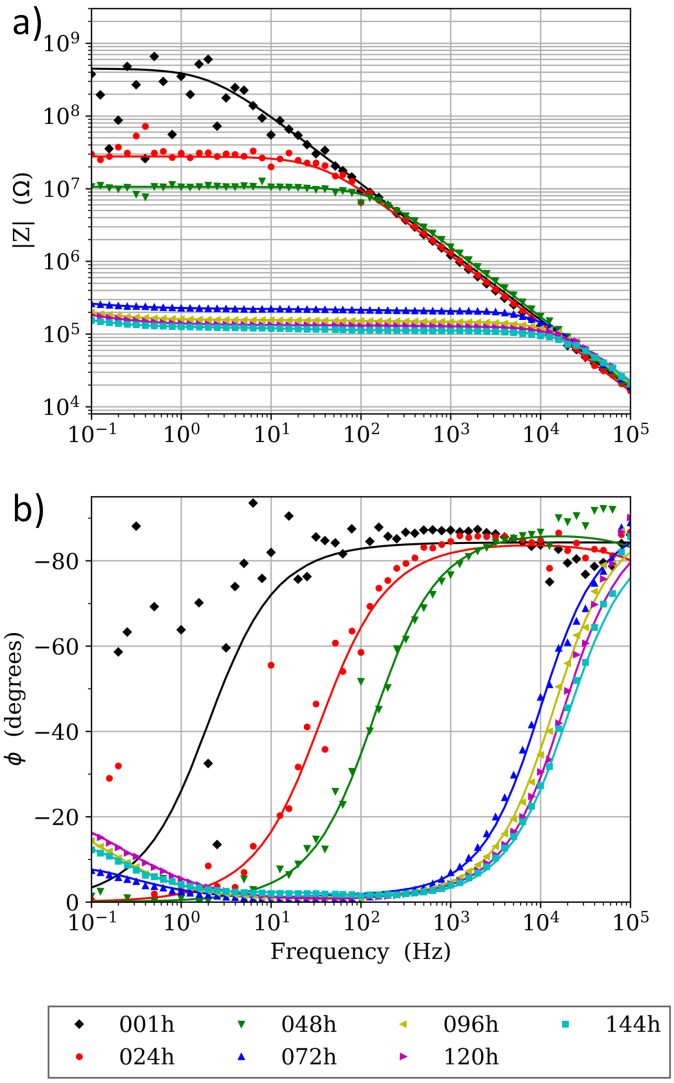

Figure 2: Impedance spectra acquired in the experiment carried out with one microelectrode inserted into porcine brain for 144 hours and characterised daily by EIS (setup A). Bode diagrams of the WE a) impedance modulus and b) phase. Dispersed symbols and solid lines respectively represent the measurements and the fitting computed through the opportune EEC model (see following section for details on EEC model).

After remaining inserted in the ex-vivo tissue, the electrode tip is covered by a continuous and uniform layer of biological material. This biofilm alters the transport phenomena close to the electrode and, as seen by impedance measurements, promotes charge transfer from the solution to the metal (also refer to the Section III-D for the microelectrode morphological characterization).

B. Equivalent electrical circuit model

The system evolves during the time of the experiment due to the interaction between the electrode tip and the biological tissue. Therefore, two different EECs were used to model the spectra. Measurements acquired until 48 hours

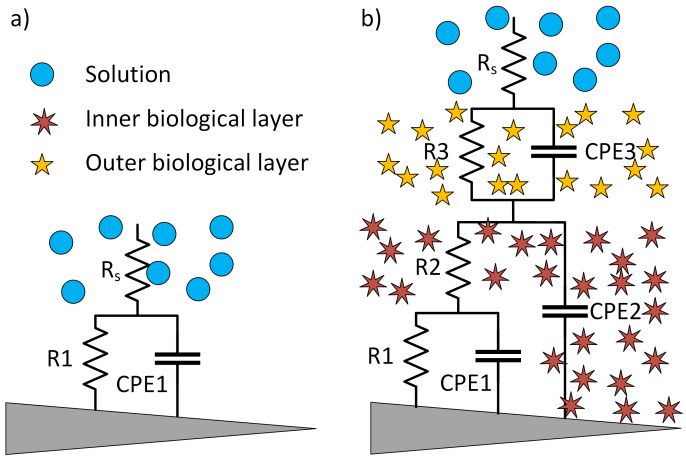

Figure 3: Equivalent Electrical Circuits (EEC) used to fit the impedance spectra acquired during the experiments. a) EEC characterised by a single time constant, used for spectra acquired up to 48 hours in contact with the porcine brain. b) EEC characterised by three time constants, used for spectra acquired in the second part of the experiment. In b), the red and yellow stars highlight two regions representing the two layers of biological materials attached on the electrode surface.

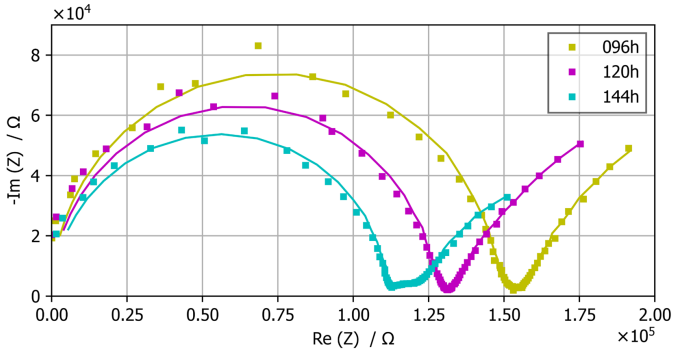

Figure 4: Nyquist diagram showing the impedance spectra of the EIS measurements at 96 h, 120 h and 144 h of the WE inserted into porcine brain for 144 hours (setup A). Dispersed squares and solid lines respectively represent the measurements and the fitting computed through the opportune EEC model.

from the electrode insertion were fitted using a single Time Constant (TC), as in Figure 3-a. The system is modeled by the electrolyte resistance (R_s) and the parallel of the double layer capacitance ($CPE1$) and the resistance to charge transfer ($R1$). In this study the capacitors were modeled as Constant Phase Elements (CPE), to take into account surface roughness and the heterogeneity characteristic of the biological samples [61, 62]. The CPE impedance Z_{CPE} is defined as follows:

$$Z_{CPE} = \frac{1}{(j\omega)^{\alpha} Q} \tag{1}$$

where j is the imaginary number, ω is the angular frequency, and Q and α are the CPE parameters.

After 48 hours a more complex model is necessary. In particular, two additional time constants appear in the spectra after 72 hours from the insertion, visible as depressed semicircles in the Nyquist plot (Figure 4). This phenomenon is related to the biological material attached to the microelectrode surface. This layer is not homogeneous and it has a variable thickness. Therefore, it can be described with a first TC ($CPE2$ and $R2$) for the inner layer (i.e. a biological layer closer to the electrode surface), and an outer layer which covers the first one (described by $CPE3$ and $R3$). The fitting quality is assessed comparing the experimental data and those derived from the EEC model. In particular, dispersed symbols and solid lines in both Figure 2-a,b and Figure 4 respectively represent the measured points and those computed using the EEC model.

The trend for all the circuit parameters above described is reported in Figure 5 for one representative sample of the experiment carried out with setup A.

The resistance to charge transfer has a decreasing trend from about $5 \cdot 10^8$ Ω to 10^7 Ω in the first two days, and then it stabilizes in the range $1 - 3 \cdot 10^5$ Ω. It is worth noting that these stationary values are more than three orders of magnitude lower than the initial one. In particular, after 72 hours, the layer of biological matter attached to the microelectrode tip becomes thicker and it can be detected by the EIS measurements. Therefore, two additional TCs have been added to the EEC to model this hetereogenous layer covering the microelectrode surface. The conditions of this biological layer are stable in the time frame investigated in these experiments, as visible by the reduced fluctuations which affect the circuit parameters related to it (Figure 5). The decreasing trend at the beginning of the experiment is attributed to the biofilm attachment on the electrode surface, which enhances the charge transfer mechanism at the interface between the electrolyte and the microelectrode. On the other hand, the values describing the double layer capacitance (i.e. Q_1 and α_1 for $CPE1$) are not deeply affected by this phenomenon, as the Pt/Ir alloy is not degraded by the interaction with the surrounding environment.

C. Impedance variation during recording - Setup B

The EEC model derived in the previous section was validated repeating the same experiment with the setup B (Figure 1-b). This experimental condition is of paramount importance for next-generation implantable neural system characterised by wireless, miniaturised and free-floating CMOS implants for neural recording.

In this experimental setup the measured impedance is the sum of two contributions: i) the interfacial impedance between the WE and the biological tissue and ii) the impedance between the tissue and the CE. Actually, in the previous setup A, due to the large area of the titanium foil, the contribution from the CE can be neglected. Instead, in this second setup B two identical microelectrodes are present and, thus, the impedance spectra are affected both by the time constants related to the WE interface and by those related to the CE interface. Consequently, the resulting model is composed by the series of two identical circuits: either the one reported in Figure 3-a (for the first part of the experiment) or the one in Figure

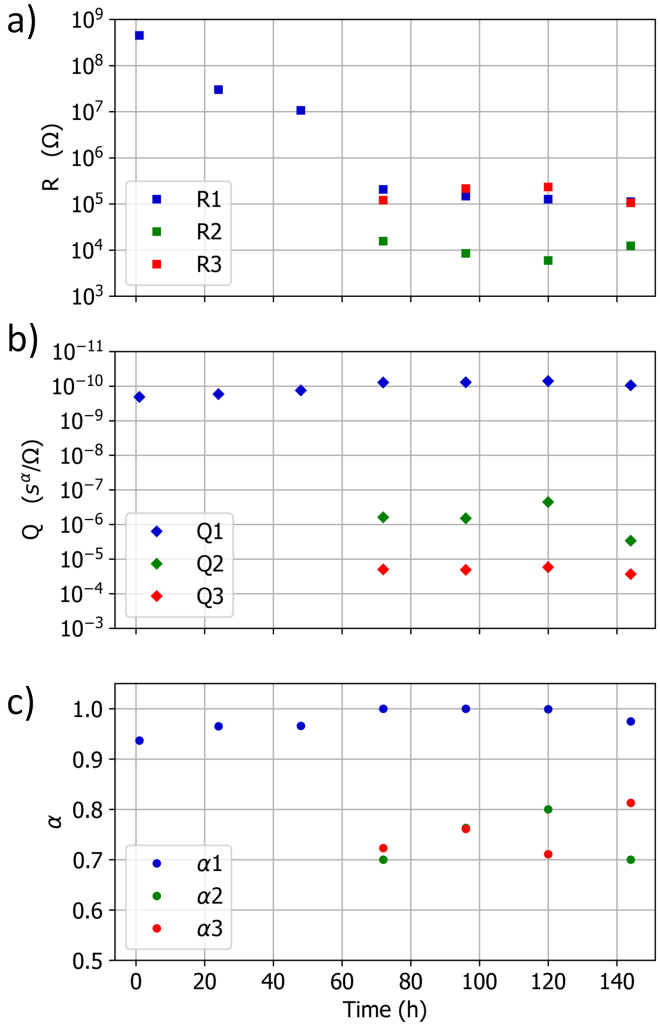

Figure 5: Trend of the different fitting parameters derived from EEC modeling of spectra acquired for one representative WE sample of the experiment conducted with setup A. a) Values of the three resistances $R1$, $R2$ and $R3$. b) Values of the three CPE parameters Q_1, Q_2 and Q_3. c) Values of the three CPE exponents α_1, α_2 and α_3. The used electrical circuit was the one shown in Figure 3-a up to 48 hours, and then the one in Figure 3-b untill the end of the experiment.

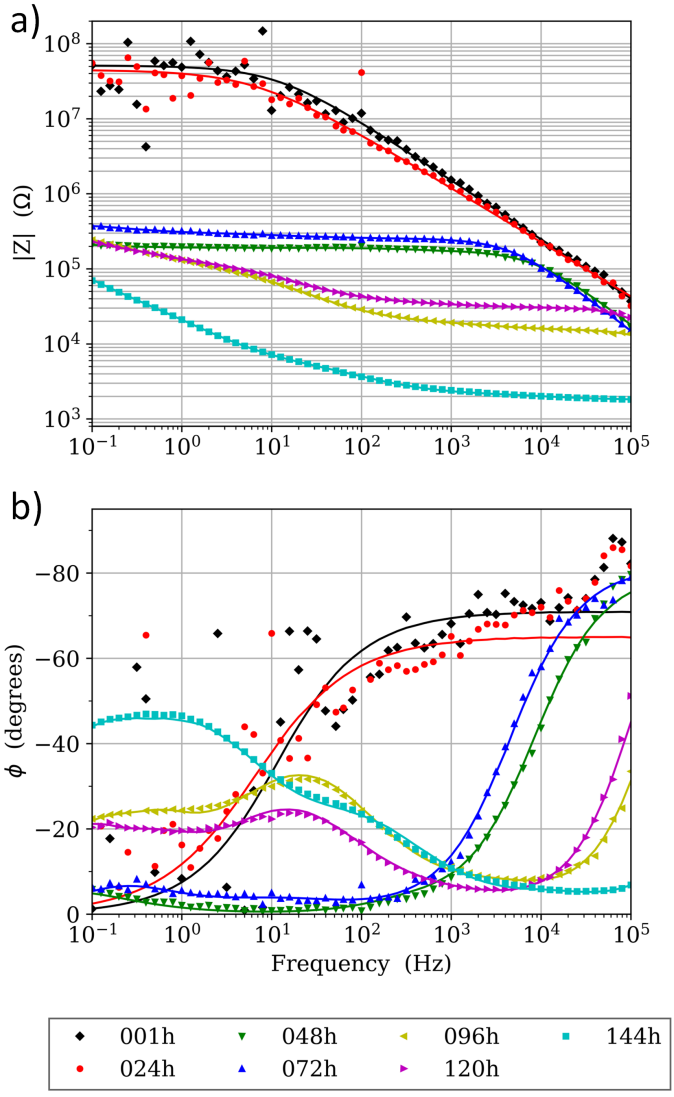

Figure 6: Impedance spectra acquired during the experiment with two identical microelectrodes inserted into porcine brain for 144 hours and characterised daily by EIS (setup B). Bode diagrams of the WE a) impedance modulus and b) phase of one sample representative of the experiment. Dispersed symbols and solid lines respectively represent the experimental data and the model computed using the opportune EEC model.

3-b (in the last part of the test). It is worth to notice that in case of two identical microelectrodes and indistinguishable phenomena on the two microelectrodes, the TCs relating to WE and CE are identical so that the poles and zeros on the Nyquist plot overlap. The global effect would be only to double the impedance magnitude, without changing the shape of the spectrum and the number of TCs. On the other hand, if the WE interfacial impedance is not identical as the one characteristic of the CE, additional features, to be modeled as TCs, would appear on the impedance spectra. As this experiment involves biological phenomena, the second condition is the one that is expected to apply.

EIS measurements acquired for one representative sample for the setup B are reported in Figure 6-a,b respectively as Bode diagrams of the electrode impedance modulus and phase. The results of the setup B highlight a much more complex interface with respect to the same experiment conducted with the setup A (Figure 2-a,b). Taking advantage of the previous findings, the appropriate model can be however applied to describe also this situation. At the beginning of the experiment, the EEC is composed only by the physical parameters related to microelectrode electrical double layer (i.e. resistance to charge transfer and double layer capacitance), thus modelled with a single TC. After 48 hours from the beginning of the test, two additional TCs appear in the impedance spectra. It is worth to notice that, as in the previous set of experiments (setup A), the appearance of additional TCs is accompanied by an

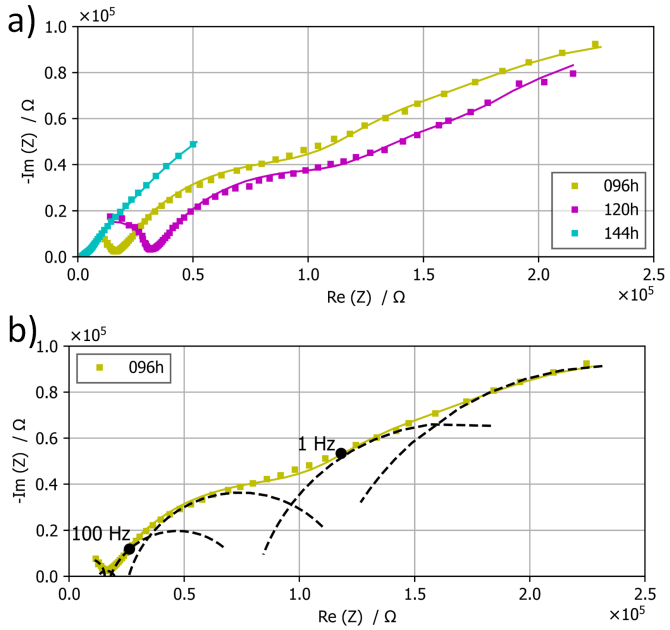

Figure 7: a) Nyquist diagram showing the impedance spectra of the EIS measurements at 96 h, 120 h and 144 h of the WE inserted into the porcine brain for 144 hours (setup B). b) Magnification of the Nyquist impedance spectra at 96 hours highlighting the six partially overlapped depressed loops corresponding to the six computed time constants (dashed semicircles). Dispersed squares and solid lines respectively represent the measurements and the fitting computed through the opportune EEC model.

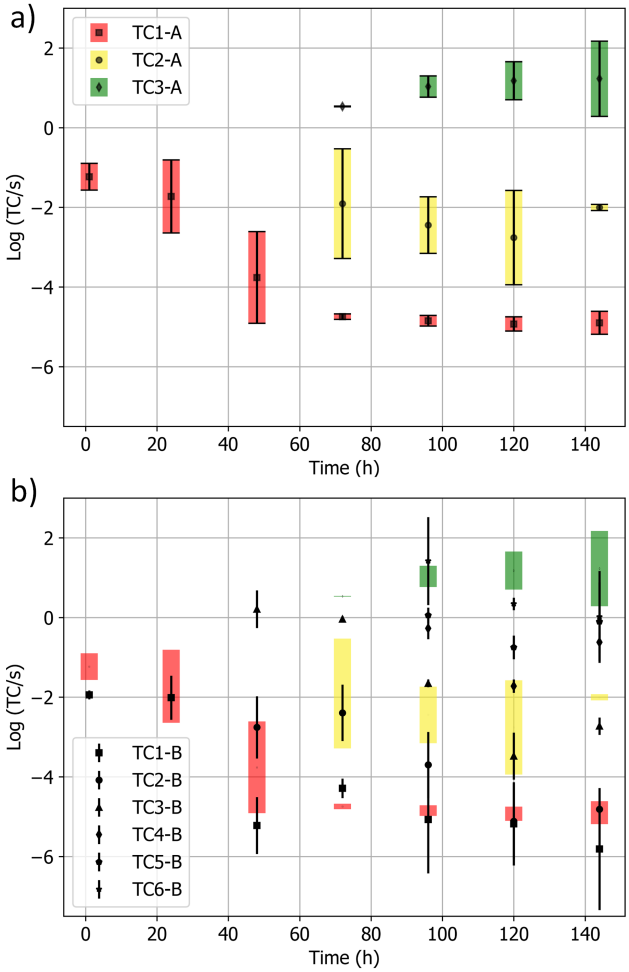

Figure 8: Evolution of time constants values during the experiments. a) Averaged time constants computed for the experiment with the setup A considering all the three investigated samples. The standard deviations for each time constant (i.e., TC1-A, TC2-A, TC3-A) are respectively reported as red, yellow, and green strips over-imposed on the standard deviation bars. b) Averaged values of the time constants computed for the experiment with the setup B (reported with their standard deviation). The same standard deviations calculated during the experiments with the setup A are reported again as red, yellow, and green strips. It is worth to notice that the calculated TCs for the experiment with the setup B (TC1-6-B) fall in the same ranges for the one with the setup A (TC1-3-A).

important reduction of the resistance to charge transfer (almost two orders of magnitude), while the double layer capacitance remains almost constant. As for the setup A, Figure 7-a shows the Nyquist plot of the EIS measurements at 96 hours, 120 hours and 144 hours for the setup B. In particular, after 96 hours, each microelectrode is covered by a thick layer of biological matter, which hinders the transport phenomena. This leads to the formation of six partially overlapped depressed loops in the Nyquist diagrams, highlighted in the Nyquist diagram of Figure 7-b by the six dashed semicircles. The first three TCs are used to model the features in the impedance plot at frequencies higher than 100 Hz. Then, three additional TCs are needed to fit the other part of the spectrum.

Thus, in order to model these spectra, two identical circuits are connected in series (each circuit is the one reported in Figure 3-b). In this way, six TCs are taken into consideration. As discussed for the previous setup, for each microelectrode, one TC describes the resistance to charge transfer and the double layer capacitance, while two TCs describe the electrochemical behavior of the biofilm. In an ideal case, half of the six TCs arise from the WE interface and the other half from the CE interface. In reality, as previously mentioned, the phenomena are indistinguishable and cannot be univocally attributed to one of the two microelectrodes. Moreover, in the case of similar TCs values for the two electrodes, a single TC will describe the phenomeon. This explains why the model contains three TCs for the measurements at 48 hours and 72 hours. In those cases a single TC models the electrical double layer of both the WE and the CE.

As the investigated phenomena of setup B are the same of setup A, they should be described by the same EECs derived from the experiment conducted with the setup A. This is further confirmed by calculating the values of the different time constants for the experiment conducted with setup A and B (Figure 8-a,b respectively). As all capacitors were modeled using CPE, the TC is calculated as in (2) [63, 64]:

$$TC_i = (R_i \cdot Q_i)^{1/\alpha_i} \quad (2)$$

where R_i is the parallel resistance and Q_i and α_i have the same meaning as in (1) for the i-time constant.

In the experiment carried out with the setup A (Figure 8-a) only a single TC is present until 48 hours from the beginning of the experiment (TC1-A, corresponding to the parallel of $R1$ and $CPE1$). Starting from 72 hours, two additional time constants appear in the spectra (TC2-A and TC3-A), which describe the biological layers accumulating on the electrodes surface. The three TCs found with the setup A describe different phenomena, and consequently are visible at different numerical scales: TC1-A at about 10^{-5} s, TC2-A in the range of 10^{-2} s, and TC3-A at about 10 s. As also described by previous literature, the phenomena involving biofilm (TC2-A and TC3-A) are those which require longer time to take place and thus are visible at lower frequency [65, 66, 67]. Additionally, it is worth to notice that our obtained TCs values are in good agreement with previous studies involving electrochemical ex-vivo characterisation for a different goal (i.e., analysing the properties of biological tissues) [55]. The latter investigated the frequency range from 1 kHz to 1 MHz and the authors found a relaxation time constant at 10^{-6} s (not visible in the frequency range analysed in the present study) and a second one at about 10^{-5} s, supporting our findings.

In the experiment with the setup B (Figure 8-b), the trend for TCs values is similar, even if their number is higher. Until 48 hours the impedance spectra are affected only by the electrical double layer, described by $CPE1$ and $R1$. Then, starting from 48 hours, two additional TCs appear in the spectra (TC2-B and TC3-B), which describe the biological layers accumulating on the electrodes surface. After 96 hours from the beginning of the experiment, both WE and CE are covered by a thick layer of biological matter, which leads to the presence of six TCs in total, associated in part to the WE and in part to the CE. Specifically, two TCs are visible at high frequencies (TC1-B and TC2-B values are below 10^{-4} s), one TC is at intermediate frequencies (TC3-B values are in the range from 10^{-4} s to 10^{-2} s) and three TCs are at low frequencies (TC4-B, TC5-B, and TC6-B values are above 10^{-1} s).

Considering both the average value and the corresponding standard deviation, the six time constants in the EEC model associated to the setup B fall in the same time intervals of the three TCs calculated for the experiment with the setup A (the standard deviation is represented in both the Figure 8-a and b as red, yellow, and green strips). Thus, the six TCs found with the setup B are describing the same phenomena of the setup A, but with a higher number of interfaces. Indeed, when six time constants are present, the TCs falling in the same range of TC1-A are associated to the microelectrodes electrical double layers (TC1-B and TC2-B), those in the range of TC2-A model the inner layer of biofilm (TC3-B and in some cases TC4-B), while the TCs in the range of TC3-A describe the outer layer of biofilm covering the two tips (TC4-B, TC5-B, and TC6-B).

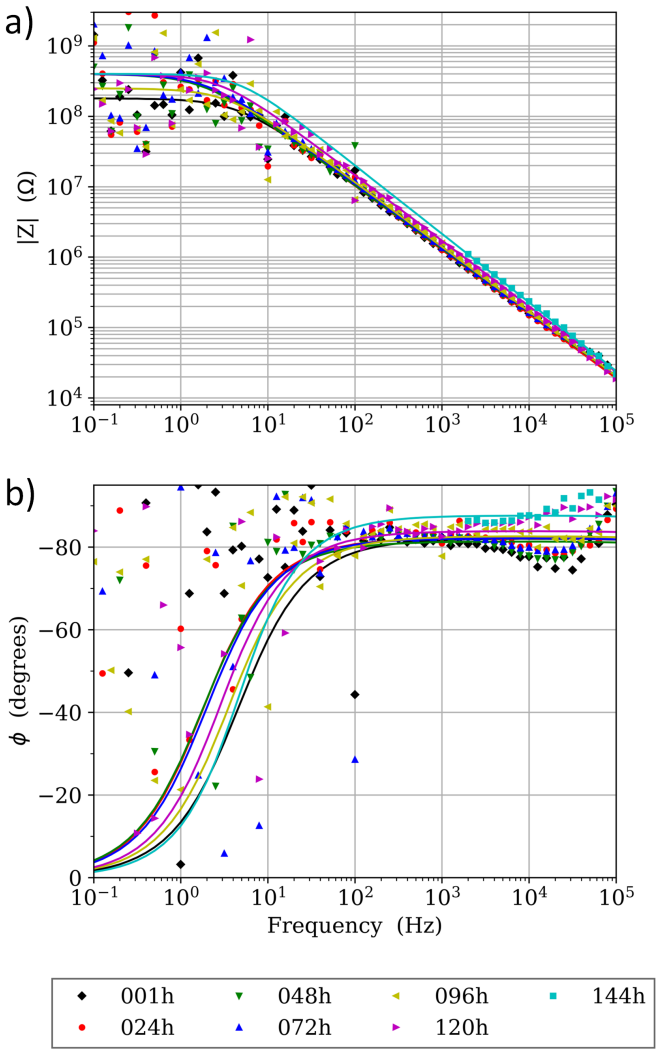

Figure 9: Impedance spectra acquired in the experiment carried out with one microelectrode inserted into porcine brain, stimulated every 24 hours and explanted after 144 hours. Bode diagrams of the WE impedance a) modulus and b) phase. Dispersed symbols and solid lines respectively represent the measurements and the fitting computed through the opportune EEC model.

D. Chronic Stimulation - Setup A

All the findings describe the electrode/brain interface impedance variation which occurs with microelectrodes inserted into the brain tissue for 144 hours: relevant case for a neural implant performing continuous neural recording. The robustness of our proposed EEC model has been proved in both the used setups. As previously discussed, the electrode/brain interface is affected by charge injection. The latter is capable to remove biological material from the microelectrode interface, thus, resulting in a cleaning effect on the microelectrode. Therefore, setup A has been chosen to investigate the effect of chronic neurostimulation on the electrode/brain interface impedance. As the impedance decrease was attributed to the biofilm accumulating on the microelectrode surface, the

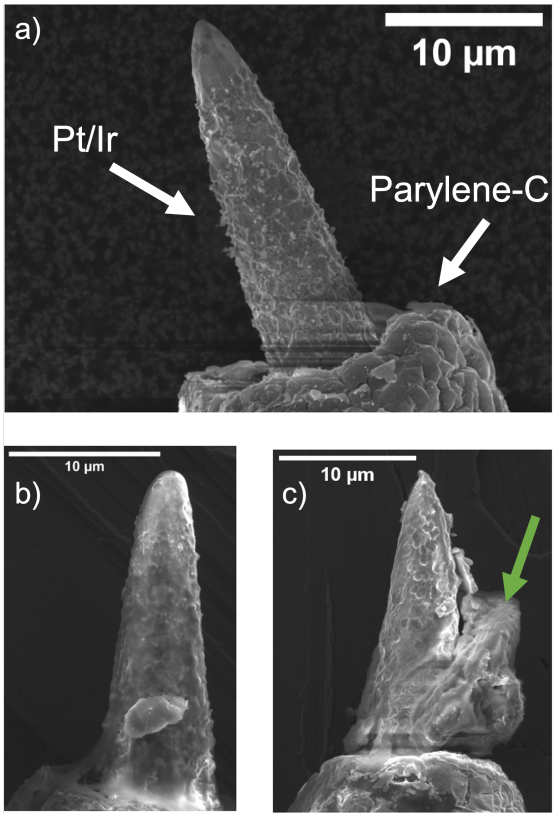

Figure 10: SEM image of the WE morphology a) before the beginning of the experiment with setup A; b) after remaining inserted into porcine brain for 144 hours (recording case); c) after remaining inserted into porcine brain for 144 hours and applying the stimulation protocol every 24 hours (chronic stimulation case). The biofilm surrounding the entire microlectrode is removed by the stimulation. The microelectrode original superficial roughness is again visible in c) and proves the cleaning effect attributed to the stimulation pattern.

cleaning effect due to the stimulation should have an opposite behaviour in the EIS spectra. In particular, the microelectrodes were stimulated continuously for one hour every 24 hours until the end of the experiment (i.e., 144 hours). EIS measurements were acquired every 24 hours and also one hour after the end of the stimulation protocol (Figure 1-c).

In all the investigated samples, impedance measurements showed no significant changes in the system. The impedance modulus remains close to the initial values until the end of the experiments (Figure 9-a). Moreover, from the phase values (Figure 9-b), a single time constant is present in the spectra for the entire duration of the experiment. As previously discussed, the noise present at low frequencies is related to the low signal to noise ratio in the measurement for high impedance values. This behaviour is thus attributed to the cleaning effect on the microelectrode surface due to the stimulation. Because of this, the biofilm does not accumulate on the Pt/Ir tip and, therefore, the impedance spectra remain essentially unaltered.

Globally, the results obtained with the EIS analysis are further supported by the morphological characterisation using the SEM. At the end of each experiment, the tip of the microelectrodes was analysed using electron microscopy. Figure 10 compares the microelectrodes tip characteristic of the different experimental conditions. Before the insertion in the biological tissue, the microelectrode tip presents its characteristic superficial roughness typical of the alloy and of the production technique (Figure 10-a).

After remaining inserted into the ex-vivo tissue for 144 hours (neural recording case), the electrode tip gets covered by a layer of biological material (Figure 10-b). As known from studies about the interaction between metals and microorganisms, biofilm formation is an accumulation process in which microorganisms produce the Extracellular Polymeric Substance (EPS), which allows them to attach to the metal surface and survive even in harsh environments [59]. This morphological observation confirms the presence of the biofilm layer predicted in the EEC model and supports the link with the impedance modulus drop occurring during the test.

Figure 10-c shows the microelectrode tip of one sample stimulated every day for 144 hours (chronic stimulation case). In this case, no additional TCs were found in the impedance spectra and, indeed, the tip superficial morphology remains almost unaltered. In particular, the microelectrode original superficial roughness is visible in almost the whole electrode tip after the experiment. A relatively large fragment of biological material (belonging to the surrounding tissue - highlighted by the green arrow in Figure 10-c) remained attached to the base of the electrode tip during extraction. This is due to fact that intense cleaning of the samples before SEM observation was intentionally avoided. As previously discussed, the microelectrode cleaning mechanism is attributed to the ability of current pulses to remove the biological material attached on metal surfaces, as already shown [17, 20, 21]. The biofilm removal by current pulses prevents the impedance drop caused by biofilm attachment [68].

In conclusion, the good agreement between the measurements acquired in the two setups confirms the validity and the robustness of the proposed models and thus allows using the EECs in Figure 3 to describe the interface between the microelectrodes and the neural tissue when designing CMOS circuits which are interfaced with the brain for both recording and stimulation.

Monitoring changes over time in the impedance of the electrode/brain interface is crucial for accurate recording and analysis of neuronal activity. Specifically, a decrease in the resistance to charge transfer results in an overall reduction in the impedance of the electrode/brain interface. In neural recording, it is essential to maintain a stable and high impedance to improve the signal-to-noise ratio and ensure high-quality recordings. Any observed changes in impedance can have a significant impact on the performance of the recordings and the quality of the signals obtained. Therefore, circuits to monitor the electrode/brain impedance are usually needed and suggested to quantify the changes over time in the impedance and to iteratively adjust the recording parameters accordingly [69]. However, in the case of neurostimulation, the impedance decrement effect is hindered by the charge injection. Therefore, if the same microelectrodes are employed for both recording and stimulation purposes, fluctuations in the

impedance of the electrode/brain interface over time become less significant. Implementing a neural recording protocol that incorporates neurostimulation would stabilize the impedance characteristics of the electrode/brain interface and facilitate optimal conditions for accurate recordings. In such cases, stimulation would only serve to clean the microelectrode from biological material, regardless of whether the device is designed to stimulate the brain for therapeutic purposes. However, it is important to ensure that the stimulation protocol used to clean the electrode does not have any negative impact on the surrounding neural tissue, as it could interfere with normal brain function, alter neural function or even cause damage. Therefore, to pursue this approach, it is necessary to investigate and optimize the stimulation protocol in order to effectively clean the electrode without affecting neural function. This involves testing different stimulation parameters, such as frequency, amplitude, and pulse width, to determine the optimal settings for cleaning while minimizing the potential for negative side effects, which is not the objective of this paper.

Last but not least, it is worth to remember that the presented study relies on ex-vivo experiments. Although the formation of the conditioning layer in the electrode/brain interface is observed in these experiments, ex-vivo studies lack active blood flow, constant plasma extravasation, and physiological micromotion. Therefore, other phenomena such as the encapsulation [20, 19] can only be analyzed thorugh in-vivo experiments. On the other hand, the great advantage of ex-vivo studies is to allow researchers to perform in an easy way a higher number of repetitions for each experimental condition.

IV. Conclusion

This study presented the electrochemical characterisation of microelectrodes for intracortical neural recording and stimulation. Ex-vivo experiments were conducted to establish appropriate electrical equivalent circuits to model the electrode/brain interface.

The results showed that for a single microelectrode, a single time constant is present during the initial stages of the experiment. However, after 72 hours from insertion into the porcine brain, biofilm accumulation at the electrode/brain interface leads to the appearance of two additional time constants in the impedance spectra. The same trend was observed in the setup constituted of two identical microelectrodes, where changes in impedance reflected the processes occurring on both the microelectrodes, leading to a doubled number of time constants. Instead of static models, we proposed non-stationary electrical equivalent circuit models whose parameters are changing over time.

In particular, when using a microelectrode mainly for neural recording it is crucial to take into account the reduction of the electrode/brain interface impedance to obtain accurate recordings of brain activity. However, if the same electrode is utilized for neurostimulation, this effect is mitigated as the charge injection removes the biological material. Indeed, the study revealed the cleaning effect caused by the applied neurostimulation protocol through electrochemical measurements and morphological characterization.

The obtained results are of paramount importance during the CMOS design of the amplifiers for neural recording, voltage or current drivers for neurostimulation and potentiostats for electrochemical sensing.

In conclusion, using the most adequate electrical equivalent circuit for the electrode/brain interface allows the design of robust circuits for interfacial impedance monitoring, for stable charge injection and, therefore, for efficient therapy.

V. Acknowledgement

This work was partially supported by the Interdisciplinary Seed Fund from École Polytechnique Fédérale de Lausanne. The Authors would like to thank the GMEE Association (Gruppo Misure Elettriche ed Elettroniche) for supporting this research by means of the 'Massimo d'Apuzzo' fellowship, granted to Dr. Leonardo Iannucci in 2020.

References

[1] A. Obaid et al. "Massively parallel microwire arrays integrated with CMOS chips for neural recording". In: *Science Advances* 6.12 (2020), eaay2789.

[2] P. Ruther and O. Paul. "New approaches for CMOS-based devices for large-scale neural recording". In: *Current opinion in neurobiology* 32 (2015), pp. 31–37.

[3] S. Carrara. "Bio/CMOS Interfaces in Voltage Scan". In: *Bio/CMOS Interfaces and Co-Design*. Springer, 2013, pp. 207–224.

[4] C. A. Rusinek et al. "All-diamond microfiber electrodes for neurochemical analysis". In: *Journal of the Electrochemical Society* 165.12 (2018), G3087–G3092.

[5] B. Bozorgzadeh et al. "Neurochemostat: A neural interface SoC with integrated chemometrics for closed-loop regulation of brain dopamine". In: *IEEE transactions on biomedical circuits and systems* 10.3 (2015), pp. 654–667.

[6] D. K. Piech et al. "A wireless millimetre-scale implantable neural stimulator with ultrasonically powered bidirectional communication". In: *Nature Biomedical Engineering* 4.2 (2020), pp. 207–222.

[7] G. J. Suaning and N. H. Lovell. "CMOS neurostimulation ASIC with 100 channels, scaleable output, and bidirectional radio-frequency telemetry". In: *IEEE Transactions on Biomedical Engineering* 48.2 (2001), pp. 248–260.

[8] W. M. Grill and J. Thomas Mortimer. "Electrical properties of implant encapsulation tissue". In: *Annals of biomedical engineering* 22.1 (1994), pp. 23–33.

[9] X. Chen et al. "Shape perception via a high-channel-count neuroprosthesis in monkey visual cortex". In: *Science* 370.6521 (2020), pp. 1191–1196.

[10] B. W. Corrigan et al. "View cells in the hippocampus and prefrontal cortex of macaques during virtual navigation". In: *Hippocampus* (2023).

[11] E. Fernández et al. "Visual percepts evoked with an intracortical 96-channel microelectrode array inserted in human occipital cortex". In: *The Journal of clinical investigation* 131.23 (2021).

[12] A. R. Harris et al. "Charge injection from chronoamperometry of platinum electrodes for bionic devices". In: *Journal of the Electrochemical Society* 165.12 (2018), G3033–G3041.

[13] D. R. Kipke et al. "Silicon-substrate intracortical microelectrode arrays for long-term recording of neuronal spike activity in cerebral cortex". In: *IEEE transactions on neural systems and rehabilitation engineering* 11.2 (2003), pp. 151–155.

[14] M. Mierzejewski et al. "The noise and impedance of microelectrodes". In: *Journal of Neural Engineering* 17.5 (2020), p. 052001.

[15] T. Wagner et al. "Biophysical foundations underlying TMS: setting the stage for an effective use of neurostimulation in the cognitive neurosciences". In: *cortex* 45.9 (2009), pp. 1025–1034.

[16] M. Dümpelmann. "Early seizure detection for closed loop direct neurostimulation devices in epilepsy". In: *Journal of neural engineering* 16.4 (2019), p. 041001.

[17] R. Eleopra et al. "Brain impedance variation of directional leads implanted in subthalamic nuclei of Parkinsonian patients". In: *Clinical Neurophysiology* 130.9 (2019), pp. 1562–1569. DOI: 10.1016/j.clinph.2019.06.001.

[18] S. F. Lempka et al. "Current-controlled deep brain stimulation reduces in vivo voltage fluctuations observed during voltage-controlled stimulation". In: *Clinical Neurophysiology* 121.12 (2010), pp. 2128–2133.

[19] C. Wang et al. "Characteristics of electrode impedance and stimulation efficacy of a chronic cortical implant using novel annulus electrodes in rat motor cortex". In: *Journal of Neural Engineering* 10.4 (2013). DOI: 10.1088/1741-2560/10/4/046010.

[20] S. F. Lempka et al. "In vivo impedance spectroscopy of deep brain stimulation electrodes". In: *Journal of neural engineering* 6.4 (2009), p. 046001.

[21] C.R. Keese et al. "Electrical wound-healing assay for cells in vitro". In: *Proceedings of the National Academy of Sciences of the United States of America* 101.6 (2004), pp. 1554–1559. DOI: 10.1073/pnas.0307588100.

[22] G. L. Barbruni et al. "Miniaturised wireless power transfer systems for neurostimulation: A review". In: *IEEE Transactions on Biomedical Circuits and Systems* 14.6 (2020), pp. 1160–1178.

[23] A. Khalifa et al. "The microbead: A 0.009 mm 3 implantable wireless neural stimulator". In: *IEEE transactions on biomedical circuits and systems* 13.5 (2019), pp. 971–985.

[24] J. Lee et al. "Neural recording and stimulation using wireless networks of microimplants". In: *Nature Electronics* 4.8 (2021), pp. 604–614.

[25] G. L. Barbruni, D. Ghezzi, and S. Carrara. "Challenges for miniaturised neurostimulators". In: *IEEE Solid-State Circuits Magazine* (2023). DOI: 10.1109/MSSC.2023.3246004.

[26] E.T. McAdams and J. Jossinet. "Tissue impedance: a historical overview". In: *Physiological measurement* 16.3A (1995), A1.

[27] K. R. Foster and H. P. Schwan. "Dielectric properties of tissues". In: *CRC handbook of biological effects of electromagnetic fields* (2019), pp. 27–96.

[28] E. Hernández-Balaguera, H. Vara, and J. L. Polo. "Identification of capacitance distribution in neuronal membranes from a fractional-order electrical circuit and whole-cell patch-clamped cells". In: *Journal of the Electrochemical Society* 165.12 (2018), G3104–G3111.

[29] A. Bagheri et al. "Low-Frequency Noise and Offset Rejection in DC-Coupled Neural Amplifiers: A Review and Digitally-Assisted Design Tutorial". In: *IEEE Transactions on Biomedical Circuits and Systems* 11.1 (2017), pp. 161–176. DOI: 10.1109/TBCAS.2016.2539518.

[30] A. Burton et al. "Wireless, battery-free, and fully implantable electrical neurostimulation in freely moving rodents". In: *Microsystems & nanoengineering* 7.1 (2021), pp. 1–12.

[31] G. L. Barbruni et al. "Ultra-Miniaturised CMOS Current Driver for Wireless Biphasic Intracortical Microstimulation". In: *2022 11th International Conference on Modern Circuits and Systems Technologies (MOCAST)*. IEEE. 2022, pp. 1–4.

[32] S. Kumar, A. Ghosh, and R. Bandyopadhyay. "Parameter estimation of Randles model of electronic tongue using system identification". In: *2019 IEEE International Symposium on Olfaction and Electronic Nose (ISOEN)*. IEEE. 2019, pp. 1–4.

[33] A. Y. Wang et al. "A Multimodal and Multifunctional CMOS Cellular Interfacing Array for Digital Physiology and Pathology Featuring an Ultra Dense Pixel Array and Reconfigurable Sampling Rate". In: *IEEE Transactions on Biomedical Circuits and Systems* (2022).

[34] M. Simić et al. "Parameter Estimation of the Randles Equivalent Electrical Circuit Using Only Real Part of the Impedance". In: *IEEE Sensors Journal* 23.5 (2023), pp. 4922–4929.

[35] K. Shen et al. "Translational opportunities and challenges of invasive electrodes for neural interfaces". In: *Nature Biomedical Engineering* (2023), pp. 1–19.

[36] K. A. Sillay et al. "Long-term measurement of impedance in chronically implanted depth and subdural electrodes during responsive neurostimulation in humans". In: *Brain stimulation* 6.5 (2013), pp. 718–726.

[37] A. T. Lenis et al. "Patterns of hardware related electrode failures in sacral nerve stimulation devices". In: *The Journal of urology* 190.1 (2013), pp. 175–179.

[38] M. D. Johnson, K. J. Otto, and D. R. Kipke. "Repeated voltage biasing improves unit recordings by reducing resistive tissue impedances". In: *IEEE Transactions on neural systems and rehabilitation engineering* 13.2 (2005), pp. 160–165.

[39] J. C. Williams et al. "Complex impedance spectroscopy for monitoring tissue responses to inserted neural implants". In: *Journal of neural engineering* 4.4 (2007), p. 410.

[40] K. Badstübner et al. "Impedance detection of the electrical resistivity of the wound tissue around deep brain stimulation electrodes permits registration of the encapsulation process in a rat model". In: *Journal of Electrical Bioimpedance* 8.1 (2017), pp. 11–24. DOI: 10.5617/jeb.4086.

[41] D. Satzer et al. "Deep Brain Stimulation Impedance Decreases Over Time Even When Stimulation Settings Are Held Constant". In: *Frontiers in Human Neuroscience* 14 (2020). DOI: 10.3389/fnhum.2020.584005.

[42] D. Satzer et al. "Variation in deep brain stimulation electrode impedance over years following electrode implantation". In: *Stereotactic and Functional Neurosurgery* 92.2 (2014), pp. 94–102. DOI: 10.1159/000358014.

[43] A. Mercanzini et al. "In vivo electrical impedance spectroscopy of tissue reaction to microelectrode arrays". In: *IEEE Transactions on Biomedical Engineering* 56.7 (2009), pp. 1909–1918. DOI: 10.1109/TBME.2009.2018457.

[44] C.-W. Chiu et al. "Electrode-immune system interface monitor through neural stimulation in American cockroach (Periplaneta Americana)". In: *Electrochimica Acta* 68 (2012), pp. 81–87. DOI: 10.1016/j.electacta.2012.02.046.

[45] M. Rosa et al. "Time dependent subthalamic local field potential changes after DBS surgery in Parkinson's disease". In: *Experimental neurology* 222.2 (2010), pp. 184–190.

[46] D. B. MacManus et al. "Towards animal surrogates for characterising large strain dynamic mechanical properties of human brain tissue". In: *Brain Multiphysics* 1 (2020), p. 100018.

[47] P. Sauleau et al. "The pig model in brain imaging and neurosurgery". In: *animal* 3.8 (2009), pp. 1138–1151.

[48] C. Zhang et al. "Effects of Different Types of Electric Fields on Mechanical Properties and Microstructure of Ex Vivo Porcine Brain Tissues". In: *ACS Biomaterials Science & Engineering* (2022).

[49] D.D. Shen, A.A. Artru, and K.K. Adkison. "Principles and applicability of CSF sampling for the assessment of CNS drug delivery and pharmacodynamics". In: *Advanced Drug Delivery Reviews* 56.12 (2004), pp. 1825–1857. DOI: 10.1016/j.addr.2004.07.011.

[50] J.R. Fogh et al. "Investigating surrogate cerebrospinal fluid matrix compositions for use in quantitative LC-MS analysis of therapeutic antibodies in the cerebrospinal fluid". In: *Analytical and Bioanalytical Chemistry* 412.7 (2020), pp. 1653–1661. DOI: 10.1007/s00216-020-02403-3.

[51] S. Hooshfar, B. Basiri, and M.G. Bartlett. "Development of a surrogate matrix for cerebral spinal fluid for liquid chromatography/mass spectrometry based analytical methods". In:

Rapid Communications in Mass Spectrometry 30.7 (2016), pp. 854–858. DOI: 10.1002/rcm.7509.

[52] M.H. Maurer. "Proteomics of brain extracellular fluid (ECF) and cerebrospinal fluid (CSF)". In: *Mass Spectrometry Reviews* 29.1 (2010), pp. 17–28. DOI: 10.1002/mas.20213.

[53] O. G. Martinsen, S. Grimnes, and H. P. Schwan. "Interface phenomena and dielectric properties of biological tissue". In: *Encyclopedia of surface and colloid science* 20 (2002), pp. 2643–2653.

[54] L. Yang et al. "Ex-vivo characterization of bioimpedance spectroscopy of normal, ischemic and hemorrhagic rabbit brain tissue at frequencies from 10 Hz to 1 MHz". In: *Sensors* 16.11 (2016), p. 1942.

[55] R.G. Ramírez-Chavarría et al. "Ex-vivo biological tissue differentiation by the Distribution of Relaxation Times method applied to Electrical Impedance Spectroscopy". In: *Electrochimica Acta* 276 (2018), pp. 214–222. DOI: 10.1016/j.electacta.2018.04.167.

[56] R. Chen, A. Canales, and P. Anikeeva. "Neural recording and modulation technologies". In: *Nature Reviews Materials* 2.2 (2017), pp. 1–16.

[57] A. Khalifa et al. "Fabrication and Assembly Techniques for Sub-mm Battery-Free Epicortical Implants". In: *Micromachines* 14.2 (2023), p. 476.

[58] E.M. Hudak, J.T. Mortimer, and H.B. Martin. "Platinum for neural stimulation: voltammetry considerations". In: *Journal of Neural Engineering* 7.2 (2010), p. 026005.

[59] R. Javaherdashti. *Microbiologically Influenced Corrosion. An Engineering Insight*. 2017, pp. 1–216.

[60] B. Tuck et al. "A critical review of marine biofilms on metallic materials". In: *npj Materials Degradation* 6.25 (2022). DOI: 10.1038/s41529-022-00234-4.

[61] M.E. Orazem and B. Tribollet. *Electrochemical Impedance Spectroscopy*. 2008, pp. 1–523. DOI: 10.1002/9780470381588.

[62] X. Muñoz-Berbel et al. "Impedimetric characterization of the changes produced in the electrode-solution interface by bacterial attachment". In: *Electrochemistry Communications* 9.11 (2007), pp. 2654–2660. DOI: 10.1016/j.elecom.2007.08.011.

[63] M.E. Orazem et al. "Dielectric properties of materials showing constant-phase-element (CPE) impedance response". In: *Journal of the Electrochemical Society* 160.6 (2013), pp. C215–C225. DOI: 10.1149/2.033306jes.

[64] K. Krukiewicz et al. "Self-supporting carbon nanotube films as flexible neural interfaces". In: *Electrochimica Acta* 295 (2019), pp. 253–261. DOI: 10.1016/j.electacta.2018.10.157.

[65] J. Paredes, S. Becerro, and S. Arana. "Label-free interdigitated microelectrode based biosensors for bacterial biofilm growth monitoring using Petri dishes". In: *Journal of Microbiological Methods* 100.1 (2014), pp. 77–83. DOI: 10.1016/j.mimet.2014.02.022.

[66] A.C. Ward et al. "Identification and characterisation of Staphylococcus aureus on low cost screen printed carbon electrodes using impedance spectroscopy". In: *Biosensors and Bioelectronics* 110 (2018), pp. 65–70. DOI: 10.1016/j.bios.2018.03.048.

[67] S. Kim et al. "Rapid bacterial detection with an interdigitated array electrode by electrochemical impedance spectroscopy". In: *Electrochimica Acta* 82 (2012), pp. 126–131. DOI: 10.1016/j.electacta.2012.05.131.

[68] C. Stucky and M. A. Johnson. "Improved Serotonin Measurement with Fast-Scan Cyclic Voltammetry: Mitigating Fouling by SSRIs". In: *Journal of the Electrochemical Society* 169.4 (2022).

[69] C.-W. Huang et al. "A CMOS Synchronized Sample-and-Hold Artifact Blanking Analog Front-End Local Field Potential Acquisition Unit With ± 3.6-V Stimulation Artifact Tolerance and Monopolar Electrode-Tissue Impedance Measurement Circuit for Closed-Loop Deep Brain Stimulation SoCs". In: *IEEE Transactions on Circuits and Systems I: Regular Papers* (2023).

Leonardo Iannucci (Member, IEEE) received the M.D. in Materials Engineering in 2016 and then the PhD in Metrology in 2019 from Politecnico di Torino (Italy). Currently he is Assistant Professor with the Department of Applied Science and Technology at Politecnico di Torino. His main research fields are metals corrosion in industry and cultural heritage applications, development of innovative coatings for corrosion protection and electrochemical measurements. He is member of IMEKO (International Measurement Confederation), and since November 2021 he has the office of Scientific Secretary in the IMEKO TC24 on Chemical Measurements. Since June 2022 he is a member of the Acta IMEKO Journal Editorial Board.

Gian Luca Barbruni (Graduate Student Member, IEEE) was born in Sanremo (IM), Italy in 1995. He received both the B.Sc. and M.Sc. degrees in Biomedical Engineering from the Politecnico di Torino, Turin, Italy in 2017 and 2019 respectively. He was a Research Associate at the Department of Electronic Engineering (DET) and MiNES (Micro&Nano Electronic Systems) Laboratory at Politecnico di Torino. Actually he is conducting his PhD in Microsystems and Microelectronics (EDMI) at Ecole Polytechnique Fédérale de Lausanne. His PhD project is focused on the development of novel miniaturised neuroprosthesis device for artificial vision. His current research interests include neural prosthesis, biosensors, wireless power transfer and data communication, ultra-low-power and miniaturised CMOS integrated circuits for the development of innovative biomedical systems.

Diego Ghezzi Prof. Diego Ghezzi received his M.Sc. in Biomedical Engineering (2004) and Ph.D. in Bioengineering (2008) from Politecnico di Milano. From 2008 to 2013, he completed his postdoctoral training at Istituto Italiano di Tecnologia in Genova at the Department of Neuroscience and Brain Technologies; where he was promoted to Researcher in 2013. In 2015, he was appointed as Tenure-Track Assistant Professor of Bioengineering at the Center for Neuroprosthetics and Institute of Bioengineering of the Ecole polytechnique fédérale de Lausanne. Prof. Diego Ghezzi holds the Medtronic Chair in Neuroengineering. His laboratory is a multidisciplinary environment promoting cross-fertilization among various expertise. The laboratory brings materials science, engineering, life science, and medicine together by the convergence of physicists, engineers, neuroscientists, and ophthalmologists cooperating to accomplish innovative projects. The mission is the development of application-driven solutions based on compliant, minimally invasive, and replaceable neuroprosthetic devices for artificial vision. Ultimately, we aim at translating our research findings into clinical practice.

Marco Parvis (Fellow, IEEE) received his MS degree in electrical engineering in 1982 from the Politecnico di Torino, Italy, and a Ph.D. degree in Metrology in 1987. He is now full professor of Electronic Measurements at the Politecnico di Torino, where he was Dean of the II Faculty of Engineering, and Fellow Member of the IEEE Society on Instrumentation and Measurement. His main fields of interest are: intelligent instrumentation, application of signal processing to measurement, biomedical and chemical measurements. He is author of more than one hundred publications.

Sabrina Grassini (Senior Member, IEEE) received her M.S. degree in Chemistry in 1999 from the University of Torino, Italy, and her Ph.D. degree in Metallurgical Engineering in 2004 from Politecnico di Torino, Italy. Now she is full professor of Applied Physical Chemistry with the Department of Applied Science and Technology, Politecnico di Torino. Her researcher areas include plasma chemistry, coating deposition, sensors, corrosion and protection of metallic materials, and conservation of cultural heritage.

Sandro Carrara (F'15) is an IEEE Fellow and also the recipient of the IEEE Sensors Council Technical Achievement Award. He is faculty at the EPFL in Lausanne (CH), former professor at the Universities of Genoa and Bologna (IT). He holds a PhD in Biochemistry and Biophysics from University of Padua (IT), a Master degree in Physics from University of Genoa (IT), and a diploma in Electronics from National Institute of Technology in Albenga (IT). Along his carrier, he published 7 books with prestigious publishers such as Springer/NATURE and Cambridge University Press. He has more than 360 scientific publications and is author of 17 patents. He is Editor-in-Chief of the IEEE Sensors Journal, one of the largest journals among 220 IEEE publications, and Associate Editor of IEEE Transactions on Biomedical Circuits and Systems. He is a member of the IEEE Sensors Council and his Executive Committee. He was a member of the Board of Governors (BoG) of the IEEE Circuits And Systems Society (CASS).